ECMOR XVII
17TH EUROPEAN CONFERENCE ON THE MATHEMATICS OF OIL RECOVERY

EAGE

An Investigation into the Upscaling of Mineral Dissolution from the Pore to the Core Scale

A.N. Faris[1], J. Maes[1*], H.P. Menke[1]

[1] Heriot-Watt University

Summary

Studying the behavior of mineral dissolution has practical uses in Carbon Capture and Storage (CCS) and Improved Oil Recovery (IOR), and several numerical models are striving to simulate the process accurately. In this paper, we investigate the core-scale numerical model presented by Golfier et al. (J. Fluid Mecha., 2002), which uses the Darcy-Brinkman-Stokes (DBS) flow formulation. This model uses a simplified Kozeny-Carmen formulation and a simplified linear formulation to describe the evolution of permeability and mass exchange coefficient as a function of porosity at the core-scale, respectively. This assumption is equivalent to neglecting the impact of pore-scale non-uniform dissolution on the prediction of the dissolution processes overall behavior. However, recent pore-scale dissolution studies have observed many different dissolution regimes, which calls into question the accuracy of the assumptions in Golfier et al. (2002)'s model. To investigate the legitimacy of this assumption, we first used our inhouse pore-scale numerical simulator (GeoChemFoam) to observe the dissolution in the uniform and dominant wormhole regimes at the pore-scale, and then developed representative permeability (K) and mass exchange coefficient (α) relations derived from the pore-scale models and applied them to the core-scale model. We observed a direct impact on the model's total permeability, the time to breakthrough and the wormhole's total porosity volume, which indicates that Golfier et al (2002)'s uniform dissolution assumption cannot be directly used for predicting the evolution of dissolution under a wide range of flow and transport conditions without investigating the relations between the pore-scale and the core-scale.

Introduction

Mineral dissolution has been extensively investigated for its role in the stimulation of petroleum wells to increase rock permeability (Rowan 1959; Chang, Qu, and Frenier 2001). Several experiments on dissolution have been performed in a variety of fluid-mineral systems (Hoefner and Fogler 1988; Fredd and Fogler 1998) using limestone core samples and injection of hydrochloric acid (HCl). Wang, Hill, and Schechter (1993) investigated the effect of temperature, acid concentration, rock mineralogy and injection rate for several Indiana or Glenn Rose limestone and dolomite cores. Bazin and Abdulahad (1999) have conducted acidizing experiments using both limestone and dolomite using various acid fluids including acids in emulsion. Luquot and Gouze (2009) have experimentally quantified the porosity and permeability changes induced by injection of CO_2 into oolitic limestone samples from the Mondeville formation (Paris Basin, France). All the experiments led to the same conclusion where different flow and transport conditions led to distinct dissolution regimes including compact dissolution, wormholes and uniform dissolution.

Dissolution simulators were developed to help predict the volume of acid required to penetrate a specific formation under specified conditions and optimize oil recovery. The simplest approach employs a single wormhole model, which assumes that a cylindrical wormhole already exists (Hung, Hill, and Sepehrnoori 1989; Wang, Hill, and Schechter 1993; Huang, Zhu, and Hill 1999). This simple model gives a good understanding of the dimensionless numbers that govern the dissolution but cannot describe the ramified structure observed in the experiments. Alternatively, models based on continuum equations written at the Darcy scale have been developed (Liu et al., 1997; Liu et al. 2003). These models used the so-called Darcy-Brinkman-Stokes (DBS) approach to model the flow in both the porous media and the developing wormholes. Golfier et al. (2002) successfully applied such a model to simulate ramified wormhole formation during mineral dissolution at the core-scale and identified and characterized all the different regimes observed in experiments.

The DBS approach relies on porosity-permeability relationships that characterize the evolution of permeability, dispersivity and mass transfer coefficient as functions of the evolving local porosity during dissolution. Simplified porosity-permeability relationships such as Kozeny-Carman (Liu et al. 1997; Golfier et al. 2002) or models based on upscaling uniform dissolution in idealized geometries ("unit cell") using volume-averaging (Quintard and Whitaker 1999) can be employed, however, they lack both accurate representations of heterogeneous rock structures and the physics governing the coupling between transport and reaction at the pore-scale.

Pore-scale investigations of subsurface processes have attracted a lot of attention in the past decade (Georgiadis et al. 2013; Menke et al. 2015) and several studies have looked at the dynamics of mineral dissolution at the pore-scale (Noiriel et al. 2009; Luquot, Rodriguez, and Gouze 2014). Menke et al. (2015; 2016; 2017; 2018) imaged the dissolution dynamics during injection of CO_2-saturated brine in various carbonate rock samples. These studies were the first to observe experimentally the existence of pore-scale dissolution regimes analogous to the regimes observed at the core-scale. These observations have been confirmed by several pore-scale simulation studies (Soulaine et al., 2017; Pereira Nunes et al., 2016).

Similar to the core-scale considerations, the large variability in dissolution behaviour at the pore-scale will lead to order of magnitude differences in the output parameters. In particular, the evolution of permeability and the mass transfer coefficient of a pore-scale sample as a function of the evolving porosity during dissolution will be radically different depending on the observed pore-scale dissolution regime. Consequently, one should question if the application of simplified uniform dissolution models for these upscaled properties that assume uniform pore structure and flow behaviour are adequate to accurately simulate the full range of regimes at the core-scale and the features of the wormhole propagation.

The objectives of this work are threefold: (1) to perform numerical simulations using our inhouse OpenFoam-based pore-scale simulator, GeoChemFoam, to observe the evolution of the Hele-Shaw pore

structure during mineral dissolutions. Two simulations will be performed, one in the uniform regime, and one in the dominant wormhole regime. The evolution of permeability and mass transfer coefficient as a function of evolving porosity will be obtained from these pore-scale results and improvements to porosity-permeability models will be proposed; (2) to develop a numerical model similar to Golfier's (2002) that can describe the various dissolution regimes during acid injection in a 2D Hele-Shaw porosity model at the core-scale. This model will be implemented in the open-source OpenFoam computational fluid dynamics library; (3) to evaluate the impact of using the pore-scale-based models in a core-scale simulation in the dominant wormhole regime by comparison with simplified permeability and mass transfer coefficient based on Kozeny-Carman and uniform dissolution assumptions. If the results are different, this study will have proven that an accurate model that takes into account the pore structure and/or the physics of dissolution at the pore-scale is essential for accurate modelling of dissolution at the core-scale.

Method

In this section, we present our domain geometry and the numerical models and implementation used in this work. Our pore-scale model employs GeoChemFoam (www.julienmaes.com/geochemfoam), our in house OpenFoam based pore-scale simulator. GeoChemFoam is used to calculate the evolution of permeability and mass transfer coefficient as a function of the evolving porous structure in a heterogenous pore-scale domain. Our core-scale model is a modification of the model presented in Golfier et al. (2002), but with a chemical model relevant to carbonate dissolution by acid injection rather than the analogue salt dissolution model used by Golfier et al. (2002). Our model has also been implemented in OpenFoam. A model for permeability and mass exchange coefficient evolution during dissolution based on the pore-scale simulation is implemented and the simulation results are compared to the ones obtained with a simplified Kozeny-Carman type model.

a. Geometry

Our core-scale domain is 2D and has a total size of 6×3 meters (Figure 1a). The simulations are performed on a 200×100 grids of 0.03m x 0.03m cells, which we assume can be represented by the same pore-scale structure (Figure 1b). This pore-scale domain was generated stochastically using 2D circular beads of uniform radius set on a uniform grid with a random deviation in the size and position of the beads.

In order to observe the development of wormhole, an initial perturbation of the system must be performed to overcome the numerical instabilities inherent in an entirely uniform simulation domain. This is achieved by introducing a perturbation into the permeability field. Two models are considered: one quasi-homogeneous case (Figure 2a) that is obtained by introducing a 10% variation in the permeability field and one heterogeneous model, obtained by introducing a variation of 90% (Figure 2b).

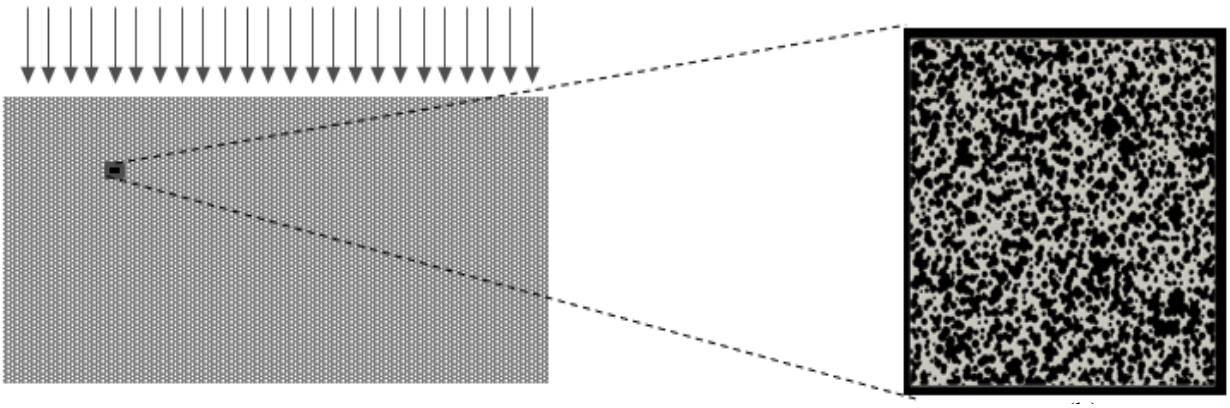

Figure 1: *Simulation domain and demonstration of the model for grid control volume*

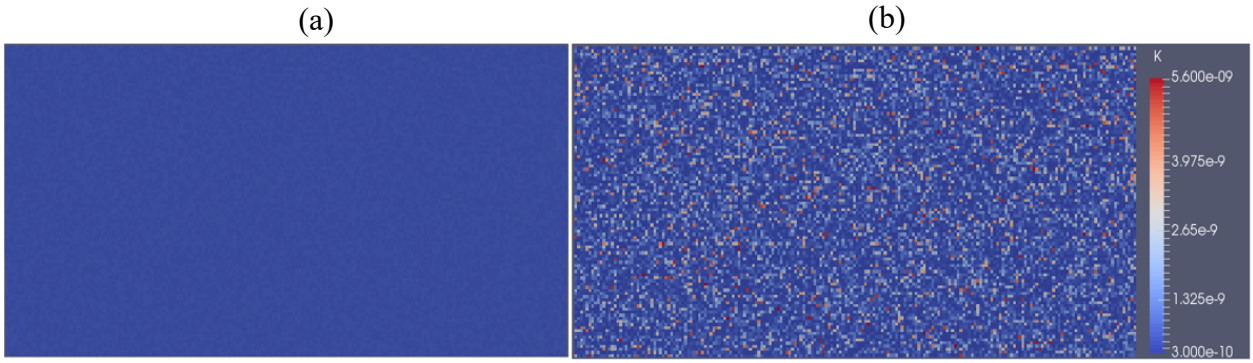

Figure 2: *Permeability distribution for the quasi-homogeneous and the heterogeneous domain*

The solid phase is assumed to be made of calcite ($CaCO_3$). Acid is injected in the domain and hydrogen ion H^+ reacts with the solid phase as follows:

$$CaCO_3 + H^+ \rightarrow Ca^{2+} + HCO_3^-. \quad (1)$$

In all core-scale simulations, the acid is injected from the top of the model, and the simulation is run until breakthrough is achieved, i.e. once the dissolution front reaches the bottom of the model. For the pore-scale simulation, the acid is injected on a side and the simulation is run until the permeability reaches a value 100 times larger than its initial value.

b. Pore-scale model

In the pore-scale model, the acid reaction with the solid phase is modelled as a boundary condition for the acid concentration in the bulk phase c_β [$k$mol. m^{-3}] at the solid interface ($A_{\beta\sigma}$):

$$-D\,\nabla c_\beta \,.\, n_{\beta\sigma} = k_c\, c_\beta \quad \text{at } A_{\beta\sigma} \quad (2)$$

here D is the molecular diffusion coefficient [m^2.s^{-1}], $n_{\beta\sigma}$ is a unit vector [-] directed at the solid phase from the fluid phase, and k_c is the reaction rate constant [m.s^{-1}] . The dissolving solid phase is receding at a velocity w [m.s^{-1}], defined by:

$$-\rho_s\, w.n_{\beta\sigma} = M_{ws} k_c\, c_\beta \quad \text{at } A\beta\sigma \quad (3)$$

where ρ_s [kg.m^{-3}] is the solid density and M_{ws} [kg.mol^{-1}] its molecular weight. The pore-scale velocity u_β [m.s^{-1}] and pressure p_β [Pa] inside the bulk phase satisfy the Stokes equation:

$$-\nabla p_\beta + \mu\,\nabla^2 u_\beta = 0, \quad (4)$$

$$\nabla \,.\, u = 0 \quad (5)$$

with no flux and no slip boundary condition at the fluid-solid interface.

$$n_{\beta\sigma} \,.\, u_\beta = 0 \quad \text{at } A_{\beta\sigma} \quad (6)$$

$$n_{\beta\sigma} \,.\, \nabla p_\beta = 0 \quad \text{at } A_{\beta\sigma} \quad (7)$$

The acid concentration solved the transport equation

$$u_\beta \,.\, \nabla c_\beta = \nabla \,.\, (D \,.\, \nabla c_\beta), \quad (8)$$

with boundary condition on the solid surface defined by Equation (**2**). The relative importance of advection, diffusion and reaction in the domain is define by the Péclet number Pe, the acid strength Na and the kinetic number Ki, defined as

$$Pe = \frac{UL}{D} \tag{9}$$

$$Ki = \frac{k_c L}{D} \tag{10}$$

$$Na = \frac{c_0 M_{ws}}{\rho_s} \tag{11}$$

where U is the injection velocity, L is a reference length and c_0 is the inlet acid concentration. The reference length is chosen as the square root of the permeability K

$$L = \sqrt{K}, \tag{12}$$

The ratio between the time scale of acid transport by diffusion in the domain and the time scale of mineral dissolution is characterized by $NaKi$ .The acid concentration is assumed to be steady-state (Equation (**8**)) during the simulation and only changes when the solid surface location changes as a result of dissolution. This assumption is valid provided that $NaKi \ll 1$.

c. Core-scale model

Our core scale model utilizes the Darcy-Brinkman-Stokes (DBS) approach to solve for the flow during the dissolution process. DBS combines Darcy's law to describe the flow in the matrix, and the Stokes equation to describe the flow in the formed channels, with the Brinkman formulation used to control continuity between the two types of cells.

The DBS approach solves for Darcy-scale volume averaged properties within a control volume. For fluid velocity, the Darcy averaged value U_β [m. s^{-1}] is given by the expression:

$$U_\beta = \langle u_\beta \rangle = \frac{1}{V_\beta} \int_{\beta-phase} u_\beta \, dV, \tag{13}$$

where V_β [m^3] is the volume of the fluid β-phase. Similarly, the Darcy averaged pressure P_β [Pa] and concentration of acid C_β [$k$mol. m^{-3}] are given by:

$$P_\beta = \langle p_\beta \rangle = \frac{1}{V_\beta} \int_{\beta-phase} p_\beta \, dV, \tag{14}$$

$$C_\beta = \langle c_\beta \rangle = \frac{1}{V_\beta} \int_{\beta-phase} c_\beta \, dV, \tag{15}$$

The reaction rate R [mol . s^{-1}] is assumed to be given by:

$$R = \alpha \, . \, C_\beta, \tag{16}$$

where α [s^{-1}] is the mass transfer coefficient. Therefore, the mineral dissolution is described by the porosity equation:

$$\frac{\partial \varepsilon}{\partial t} = \frac{M_{ws} \, \alpha \, C_\beta}{\rho_s}, \tag{17}$$

where ε[-] is the porosity.

The flow field solves the following Brinkman equation (Brinkman 1949),

$$\frac{\mu}{\varepsilon}\nabla^2 U_\beta - \nabla P_\beta - \mu K^{-1}.V_\beta = 0 \tag{18}$$

Here μ [kg. m^{-1}s^{-1}] is the viscosity and K [m^2] is the permeability. If the flow is in a wormhole, the Laplacian term becomes predominant and the flow model follows Stokes law. If the flow is in the porous matrix, Darcy flow dominates.

Like for the pore-scale model, the acid concentration in the domain is assumed to be steady-state.

$$U_\beta . \nabla C_\beta = \nabla . \left(D^* . \nabla C_\beta\right) - \alpha . C_\beta \tag{19}$$

where D^* [m^2 s^{-1}] is the dispersivity tensor. The steady-state assumption is only valid if the timescale of mineral dissolution is slow compared to the time scale of acid transport in the domain, i.e. $NaDa \ll 1$, where the Damköhler number Da is defined as

$$Da = \frac{L\alpha}{U} \tag{20}$$

Permeability, mass transfer coefficient and dispersivity are Darcy-scale properties that evolve during dissolution. In order to complete our core-scale model, they are expressed as functions of porosity. In this work, we assume that the dispersivity varies linearly with porosity, i.e.

$$D^* = \varepsilon D \tag{21}$$

For the permeability and the mass exchange coefficient, two models are implemented and compared. The first model uses Kozeny-Carman-type relationship for porosity-permeability and porosity-mass exchange coefficient dependencies

$$\mathrm{K} = \mathrm{K}_0 \left(\frac{\mathrm{X}}{X_0}\right)^n \tag{22}$$

$$\alpha = \alpha_0 \left(\frac{\mathrm{X}}{X_0}\right)^p \tag{23}$$

where

$$X = \frac{\varepsilon}{1-\varepsilon} \tag{24}$$

Kozeny-Carman-type relationship are typically applied when no information on the real pore-scale structure is available. In this work, we chose n = 3 and p = -1.

Alternatively, the evolution of permeability and the mass transfer coefficient with changes in porosity can be obtained from pore-scale simulations. The permeability of a control volume represented by a pore-scale domain is defined as:

$$K = \mu \frac{Q\, l}{\Delta P\, A} \tag{25}$$

where l [m] is the length of the domain, A [m^2] is the cross-section of the control volume, Q [m^3/s] is the flow rate, and ΔP [Pa] is the pressure drop between inlet and outlet. Q and ΔP can be calculated as:

$$Q = \int_{inlet} u_\beta . n_{inlet}\, dA, \tag{26}$$

$$\Delta P = \frac{1}{A}\left(\int_{inlet} p_\beta dA - \int_{outlet} p_\beta dA\right) \tag{27}$$

Similarly, the mass transfer coefficient in a control volume represented by a pore-scale domain is defined as

$$\alpha = \frac{\bar{R}}{C_\beta V_\beta} \tag{28}$$

where $\bar{R}$ is the total reaction rate in the pore scale domain,

$$\bar{R} = \int_{A_{\beta\sigma}} k_c\, c_\beta\, dA. \tag{29}$$

Results and Discussion

a. Pore-scale simulations

Two pore-scale numerical simulations were performed to investigate the effectiveness of porosity-permeability and mass transfer coefficients derived from pore-scale simulations. The pore-scale geometry used is shown in Figure 1b. Acid was injected from the left at constant velocities. The parameters for the pore-scale simulations are summarized in Table 1. The porosity and permeability can be numerically calculated after solving for the initial flow field and we find $\varepsilon = 0.455$ and $K = 5.65 \times 10^{-10}$ m^2 (25)). This correspond to a reference length $L = 2.38 \times 10^{-5}$ m. Therefore, the value of the parameters correspond to $Pe = 8.8 \times 10^{-2}$ and $Ki = 19.3$ for the dominant wormhole regime, and $Pe = 0.88$ and $Ki = 0.0193$ for the uniform dissolution regime.

Table 1: Parameters for pore-scale simulations of mineral dissolutions

	Dominant wormhole regime	Uniform dissolution regime
Injection velocity	3.7×10^{-6} m/s	3.7×10^{-5} m/s
Molecular Diffusion	10^{-9} m^2/s	10^{-9} m^2/s
Reaction constant	8.15×10^{-4} m/s	8.15×10^{-7} m/s
Acid concentration	0.01 $kmol.m^{-3}$	0.01 $kmol.m^{-3}$
Mineral molecular weight	100 kg/kmol	100 kg/kmol
Solid density	2700 kg.m^{-3}	2700 kg.m^{-3}

The evolution of the porous structure and the acid concentration profile is presented below in Figure 3. We observe that the evolution of the pore structure is completely different for the two dissolution regimes. This will result in very different permeability and mass exchange coefficient evolutions with dissolution.

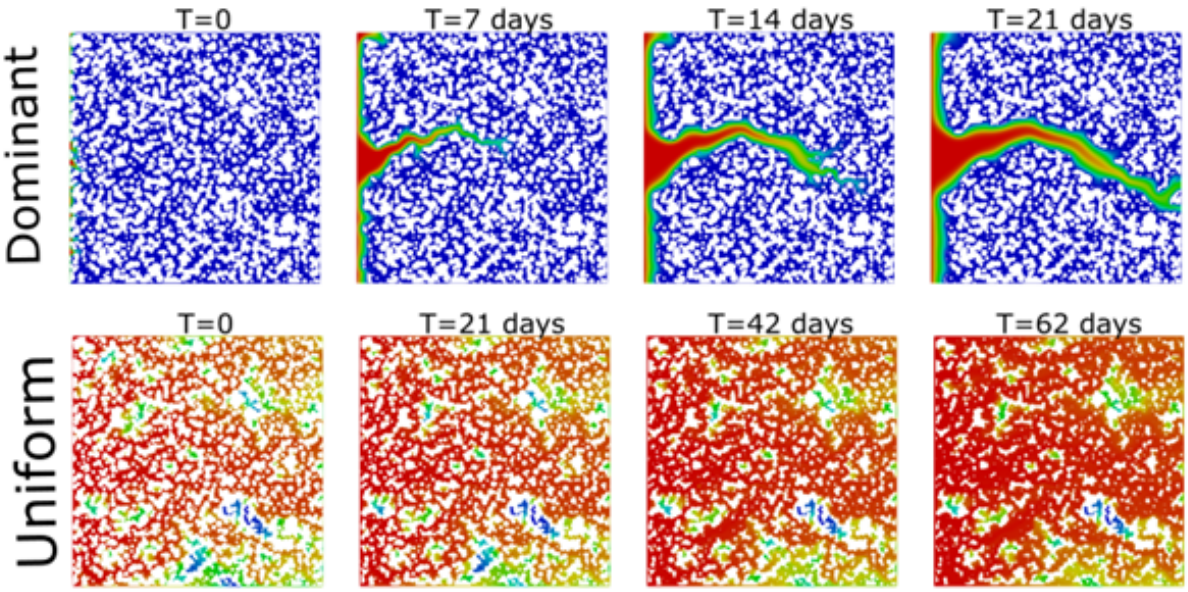

Figure 3: *Dominant wormhole and uniform dissolution regimes at the pore-scale*

The permeability-porosity and the mass transfer coefficient-porosity relationship can be calculated using Equations (**25**) and (**28**) . The results for the two pore-scale models are plotted in Figure 4. **Error! Reference source not found.**The Kozeny-Carman-type models for permeability (order 3) and mass exchange coefficient (order -1) are also plotted. We observed that these models are a good match for the pore-scale uniform dissolution model. This show that the Kozeny-Carman type models are equivalent to assume that the dissolution is uniform at the pore-scale.

In addition, the dominant wormhole model is obtained by matching trend lines to the pore-scale model. The trendlines were defined as:

$$K = \lambda_0 \, e^{\left[-\lambda_1 \times \left(\frac{eps^{\lambda_2}}{(1-eps)^{\lambda_3}}\right)\right]} \tag{30}$$

$$\alpha = \lambda_4 \left(\frac{(1-eps)}{eps}\right)^{\lambda_5} \tag{31}$$

and the coefficients λ_i were obtained by minimalizing the L_2 error. The resulting models are

$$K = K_0 \, e^{\left[-4 \times \left(\frac{eps^4}{(1-eps)^3} - \frac{eps_0{}^4}{(1-eps_0)^3}\right)\right]} \tag{32}$$

$$\alpha = \max\left[\left(\frac{eps_0}{(1-eps_0)}\,\frac{(1-eps)}{eps}\right)^{15}, \; \frac{1}{3}\left(\frac{eps_0}{(1-eps_0)}\frac{(1-eps)}{eps}\right)^{5}\right] \tag{33}$$

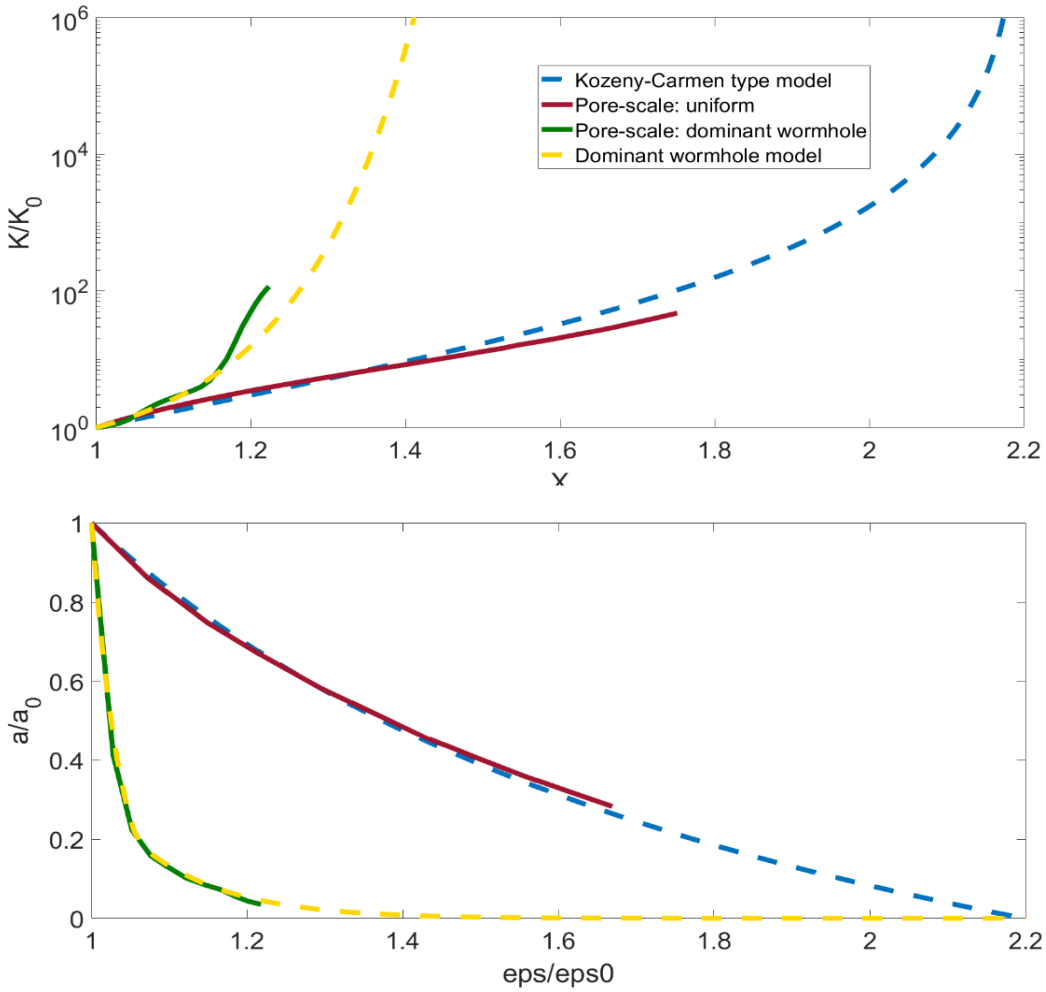

Figure 4: *Permeability and mass exchange coefficient evolution as a function of porosity during dissolution of the pore-scale domain*

b. Core-scale simulations

We now compare core-scale simulations obtained with three different upscaling models for the permeability and the mass exchange coefficient. These dissolution models are:

A. Kozeny-Carman-type relations for permeability and mass transfer coefficient
B. Pore-scale dominant wormhole model for permeability and Kozeny-Carman-type relation for mass exchange coefficient.
C. Pore-scale dominant wormhole model for permeability and mass transfer coefficient.

Three simulations are then performed for the quasi-homogeneous and the heterogeneous models. The parameters for the simulations are presented in Table 2. The initial permeability and mass exchange coefficient were obtained from the pore-scale model using Equations (**25**) and (**28**) for the dominant wormhole pore-scale regime (Table 1). Then, their evolution is conditioned by model A, B or C.

Figure 5 show the porosity field at t=$\mathbf{1.1} \times 10^8$ s for dissolution in the quasi-homogeneous domain with the three upscaling models. The most obvious difference here is the lighter colors in model (C), which indicates a lower overall porosity, and thus less complete dissolution of the pore structure inside the wormholes when compared to dissolution models (A) and (B). At this time, Model (C) is at breakthrough but Model (A) and (B) are still forming their wormholes. This is because the mass exchange coefficient obtained using the pore-scale dominant wormhole drop much faster than the one obtained with the Kozeny-Carman-type relation.

Table 2: Parameters for core-scale simulations of mineral dissolutions

	Core-scale parameters
Injection velocity	$3.7 \times 10^{-6}\ \mathrm{m.s^{-1}}$
Molecular Diffusion	$10^{-9}\ .\mathrm{s^{-1}}$
Initial porosity	0.455
Initial permeability	$5.65 \times 10^{-10}\ \mathrm{m^2}$
Initial mass exchange coefficient	$0.02\ \ \mathrm{s^{-1}}$
Acid concentration	$0.01\ \mathrm{kmol.m^{-3}}$
Mineral molecular weight	$100\ \mathrm{kg.kmol^{-1}}$
Solid density	$2700\ \mathrm{kg.m^{-3}}$

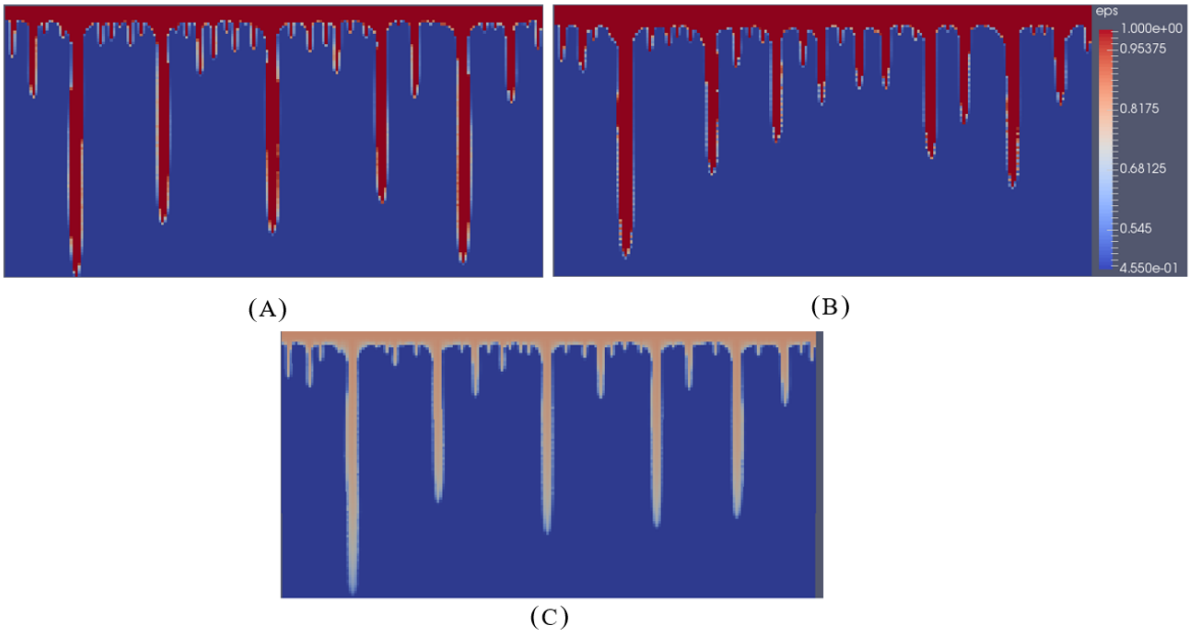

Figure 5: *Porosity field at t=*$\mathbf{1.1 \times 10^8}$*s for core-scale dissolution in the quasi-homogeneous domain using upscaling permeability and mass exchange coefficient models A, B and C*

Figure 6 **Error! Reference source not found.**shows the porosity field at breakthrough obtained with the three models. We observe that model (B) has wider wormholes that model (A). In addition, at breakthrough, there is clearly one dominant wormhole while with model (A), two wormholes have developed all the way to the boundary and three are almost there. This is because, for the same porosity, the permeability obtained using the pore-scale dominant wormhole is much larger than the one obtained using the Kozeny-Carman-type model. However, Model (C) has thinner and longer wormholes compared to dissolution Model (B), similar to the one of Model (A). This because of the incomplete dissolution, which results in a lower permeability.

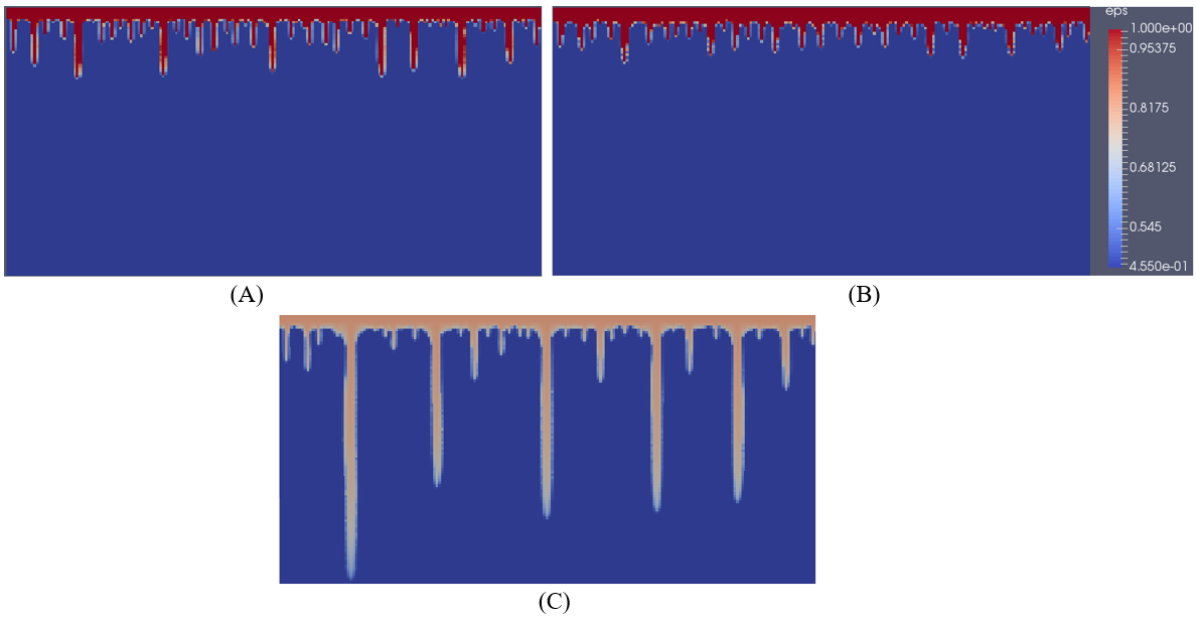

Figure 6: *Porosity field at breakthrough for core-scale dissolution in the quasi-homogeneous model using upscaling permeability and mass exchange coefficient models A, B and C*

Figure 7 shows the dissolution pattern at $t = 1.1 \times 10^8$ s for dissolution in the heterogeneous domain using the three upscaling models. Similar to the quasi-homogeneous case, we observe a less complete dissolution of the pore structure inside the wormholes leading to a much earlier breakthrough. When Model (C) is on the boundaries to breakthrough, Model (A) and (B) are still forming its wormholes.

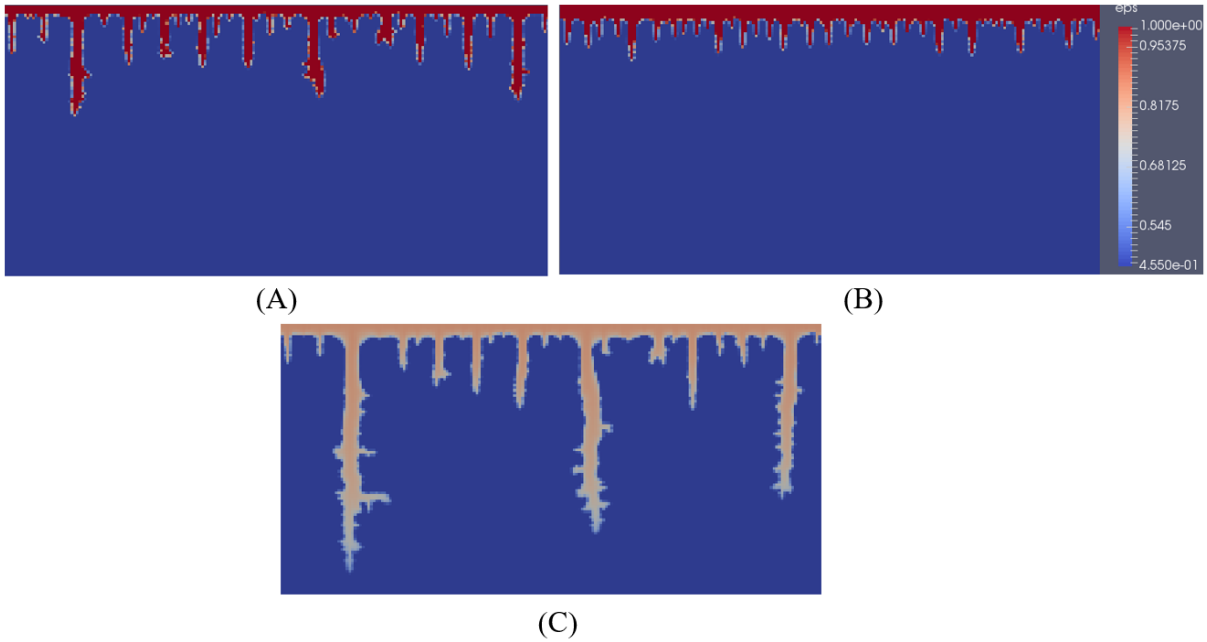

Figure 7: *Porosity field at t=$\mathbf{1.1 \times 10^8}$s for core-scale dissolution in the heterogeneous model using upscaling permeability and mass exchange coefficient models A, B and C.*

Figure 8 shows the dissolution pattern at breakthrough for the three models. We observe a lot of branching with Model (A). This is because of preferential flow paths induced by the heterogeneity. However, there is less branching in Model (B). The is because in Model (B) the permeability increases stiffly with the porosity. Indeed, the permeability has been multiplied by 100 after a change of porosity

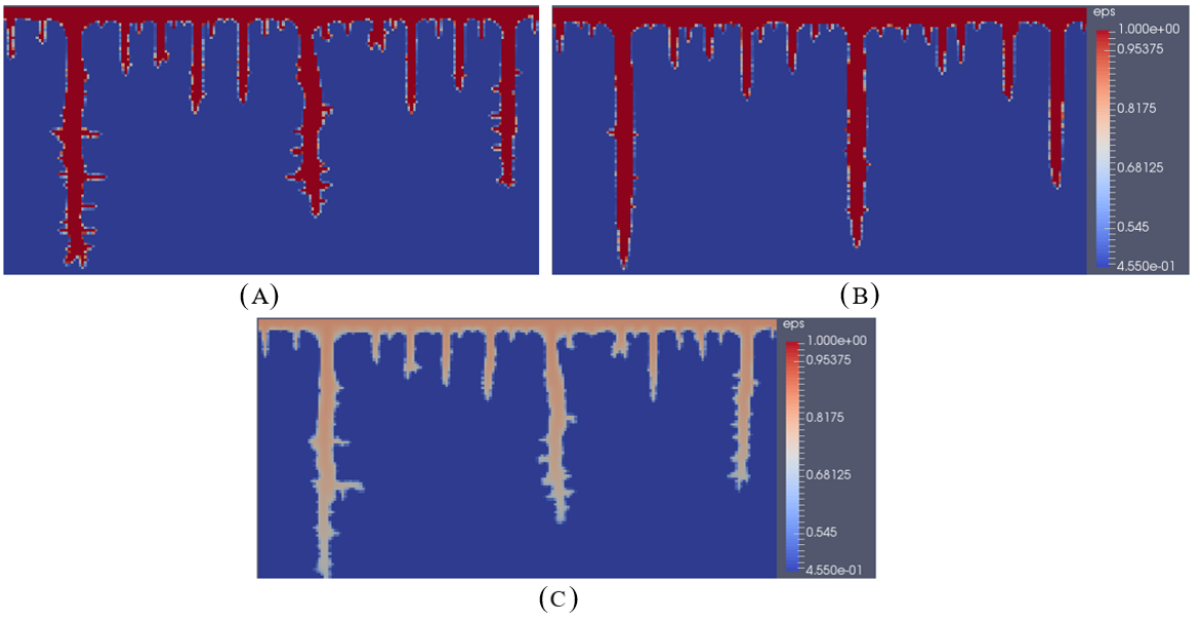

Figure 8: *Porosity field at breakthrough for core-scale dissolution in the quasi-homogeneous model using upscaling permeability and mass exchange coefficient models A, B and C*

of just 20% (Figure 4). In comparison to Model (A), the permeability perturbations are negligible, and branching is almost inexistent in Model (B). The breakthrough time is not significantly affected, although the wormholes are wider in Model (B) compared to Model (A). The wormhole branching re-appears when the mass transfer coefficient relation is added in Model (C). Here, the mass transfer coefficient decreases rapidly and the dissolution in the wormholes is not complete. Therefore, the permeability in the wormhole is much less than for Model B and the perturbations are not negligible anymore. As a result, the dissolution leads to branching in the wormholes again.

Finally, the evolution of the total permeability of the core-scale model (Figure 1a) with time for the quasi-homogeneous and heterogeneous domains, and for the three upscaling models is presented in Figure 9. For the quasi-homogeneous domain, Model (B) had a delayed breakthrough compared to Model (A) with the increase in the model's total permeability. Model (C) led to a much earlier breakthrough when compared to the other models, while maintaining the same total permeability increase as in Model (B).

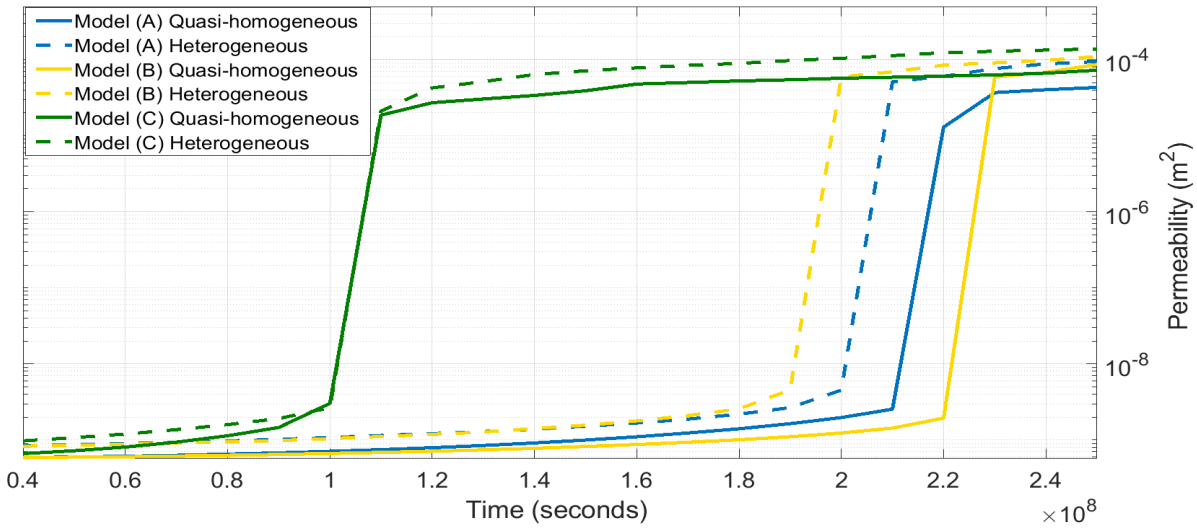

Figure 9: *Total core-scale permeability evolution during dissolution in the quasi-homogeneous and heterogeneous model, and using the three different upscaling models*

The heterogenous model had larger variations in the permeability distribution, which led to an increase in the breakthrough permeability for all dissolution models, and earlier breakthrough for dissolution Models (A) and (B), but not (C).
We also noticed that Model (B) has a later breakthrough than model (A) for the quasi-homogeneous model, but not for the heterogeneous model. This is because Model (B) led to wider wormholes in both domains, but no branching for the heterogeneous model.

Conclusions

We have investigated the influence of using alternative pore-scale expressions for the porosity-permeability relationship and mass transfer coefficients in a core-scale numerical dissolution model These new pore-scale expressions are representative of the pore-scale dominant wormhole dissolution regime and are derived from pore-scale numerical experiments that capture more representative behavior than the simple uniform dissolution expressions equivalent to using Kozeny-Carman-type relationship. We found that when upscaling from a pore-scale to core-scale dissolution model, the dissolution regime observed at the pore-scale has direct impact on the dissolution regime observed at the core-scale. We investigated the possible impacts of these different models, and we established that the porosity-permeability relationship and mass transfer coefficients change the resultant porosity and permeability, as well as the time to breakthrough of the models. Furthermore, there was an impact on the number and the shape of the wormholes formed during the dissolution simulation indicating that the boundaries between dissolution regimes are affected by these pore-scale relationships.

Moreover, we examined the results of our models in both a quasi-homogeneous domain and a heterogeneous permeability domain and found that permeability heterogeneity also impacted the dissolution process. We can therefore conclude that when using a core-scale numerical model to predict dissolution, it is essential to consider the dissolution at the pore-scale because it has a direct influence on the dissolution regime. However, the influence on dissolution characteristics was not measured for every possible flow and transport condition nor was it extended to variances in pore-scale structural heterogeneity. In addition, the pore-scale regime (dominant wormhole) was assumed to be the same everywhere in the domain, while in reality this will change dynamically with the local velocity in each cell. This will require further investigation to apply the results to more complex and multi-scale structures and is a target of future work.

This study has shown the value of incorporating pore-scale structural information into core-scale models. Our results are especially relevant to the enhanced oil recovery industry where small changes in injection strategy represent millions of dollars in potential revenue, or to CCS, where small change in the dissolution patterns can result in leakage of CO_2 out of storage reservoirs. Using new pore-scale information in these models can ultimately help optimize the injection strategies for well acidization and carbon storage projects to improve both storage and recovery.

Acknowledgement

This work was partly supported by the UK EPSRC funded project on Direct Numerical Simulation for Additive Manufacturing in Porous Media (grant reference EP/P031307/1).

References

Bazin, B. and Abdulahad, G. 1999. “Experimental Investigation of Some Properties of Emulsified Acid Systems for Stimulation of Carbonate Formations.” In *Middle East Oil Show and Conference*, 20-23 February, Bahrain.

Brinkman, H. C. 1949. "A Calculation of the Viscous Force Exerted by a Flowing Fluid on a Dense Swarm of Particles." *Flow, Turbulence and Combustion* 1 (1): 27.

Chang, F., Qu, and Frenier, W. 2001. "A Novel Self-Diverting-Acid Developed for Matrix Stimulation of Carbonate Reservoirs." In *SPE International Symposium on Oilfield Chemistry*, 13-16 February, Houston, Texas

Fredd, C. N. and Fogler, H. S. 1998. "Influence of Transport and Reaction on Wormhole Formation in Porous Media." *AIChE Journal* 44 (9): 1933–49.

Georgiadis, A., Berg, S., Makurat,, A., Maitland, G. and Ott, H. 2013. "Pore-Scale Micro-Computed-Tomography Imaging: Nonwetting-Phase Cluster-Size Distribution during Drainage and Imbibition." *Physical Review E* 88 (3): 33002.

Golfier, F., Zarcone, C., Bazin, B., Lenormand, R., Lasseux, D., and Quintard, M. 2002. "On the Ability of a Darcy-Scale Model to Capture Wormhole Formation during the Dissolution of a Porous Medium." *Journal of Fluid Mechanics* 457: 213–54.

Hoefner, M. L., and Fogler, H. S. 1988. "Pore Evolution and Channel Formation during Flow and Reaction in Porous Media." *AIChE Journal* 34 (1): 45–54.

Huang, T., Zhu, D. and Hill, A. D. 1999. "Prediction of Wormhole Population Density in Carbonate Matrix Acidizing." In *SPE European Formation Damage Conference*., 31 May-1 June, The Hague, Netherlands

Hung, K. M., Hill, A. D. and Sepehrnoori, K. 1989. "A Mechanistic Model of Wormhole Growth in Carbonate Matrix Acidizing and Acid Fracturing." *Journal of Petroleum Technology* 41 (01): 59–66.

Liu, H. and Haukwa, C. B., Ahlers, C. F., Bodvarsson, G. S., Flint, A. L. and Guertal, W. B. 2003. "Modeling Flow and Transport in Unsaturated Fractured Rock: An Evaluation of the Continuum Approach." *Journal of Contaminant Hydrology* 62: 173–88.

Liu, X., Ormond, A., Bartko, K., Ying, L., and Ortoleva, P. 1997. "A Geochemical Reaction-Transport Simulator for Matrix Acidizing Analysis and Design." *Journal of Petroleum Science and Engineering* 17 (1–2): 181–96.

Luquot, L, and Gouze, P. 2009. "Experimental Determination of Porosity and Permeability Changes Induced by Injection of CO_2 into Carbonate Rocks." *Chemical Geology* 265 (1): 148–59.

Luquot, L., Rodriguez, O., and Gouze, P. 2014. "Experimental Characterization of Porosity Structure and Transport Property Changes in Limestone Undergoing Different Dissolution Regimes." *Transport in Porous Media* 101 (3): 507–32.

Menke, H. P., Andrew, M. G., Blunt, M. J. and Bijeljic, B.. 2016. "Reservoir Condition Imaging of Reactive Transport in Heterogeneous Carbonates Using Fast Synchrotron Tomography - Effect of Initial Pore Structure and Flow Conditions." *Chemical Geology* 428: 15–26

Menke, H. P., Bijeljic, B. Blunt, M. J. 2017. "Dynamic Reservoir-Condition Microtomography of Reactive Transport in Complex Carbonates: Effect of Initial Pore Structure and Initial Brine PH." *Geochimica et Cosmochimica Acta* 204: 267–85.

Menke, H. P., Reynolds, C. A., Andrew, M. G., Pereira Nunes, J. P., Bijeljic, B., and Blunt, M. J. 2018. "4D Multi-Scale Imaging of Reactive Flow in Carbonates: Assessing the Impact of Heterogeneity on Dissolution Regimes Using Streamlines at Multiple Length Scales." *Chemical Geology* 481: 27–37.

Menke, H. P., Bijeljic, B., Andrew, M. G. and Blunt, M. J.. 2015. "Dynamic Three-Dimensional Pore-Scale Imaging of Reaction in a Carbonate at Reservoir Conditions." *Environmental Science & Technology* 49 (7): 4407–14.

Noiriel, C., Luquot, L., Madé, B., Raimbault, L., Gouze, P., and Van Der Lee, J.. 2009. "Changes in Reactive Surface Area during Limestone Dissolution: An Experimental and Modelling Study." *Chemical Geology* 265 (1–2): 160–70.

Pereira Nunes, J. P., Blunt, M. J. and Bijeljic, B. 2016. "Pore-scale simulations of carbonate dissolution in micro-CT images." J. Geophys. Res. Solid Earth. 121:558-556

Quintard, M. and Whitaker, S. 1999. "Fundamentals of Transport Equation Formulation for Two-Phase Flow in Homogeneous and Heterogeneous Porous Media." In Vadose Zone Hydrology,

Oxford University Press.

Rowan, G. 1959. "Theory of Acid Treatment of Limestone Formations." *J. Inst. Pet* 45 (431): 321.

Soulaine, C., Roman, S., Kovscek, A. and Tchelepi, H. A. 2017. "Mineral Dissolution and Wormholing from a Pore-Scale Perspective". *Journal of Fluid Mechanics* 827:457:483

Wang, Y., Hill, A. D., and Schechter, R. S. 1993. "The Optimum Injection Rate for Matrix Acidizing of Carbonate Formations." In *SPE Annual Technical Conference and Exhibition*, 3-6 October, Houston, Texas.